

# Memory-efficient Lattice Boltzmann Method for low Reynolds number flows

Maciej Matyka <sup>\*1</sup>

<sup>1</sup>*Faculty of Physics and Astronomy, University of Wrocław, pl. M. Borna 9, 50-205 Wrocław, Poland, tel.: +48713759357, fax: +48713217682*

December 20, 2019

## Abstract

The Lattice Boltzmann Method algorithm is simplified by assuming constant numerical viscosity (the relaxation time is fixed at  $\tau = 1$ ). This leads to the removal of the distribution function from the computer memory. To test the solver the Poiseuille and Driven Cavity flows are simulated and analyzed. The error of the solution decreases with the grid size  $L$  as  $L^{-2}$ . Compared to the standard algorithm, the presented formulation is simpler and shorter in implementation. It is less error-prone and needs significantly less working memory in low Reynolds number flows.

## 1 Introduction

Computational fluid dynamics (CFD) is useful in many branches of science and technology, including those related to main civilization challenges of the utmost importance for the whole society e.g. weather forecast, climate, sport, medicine, oil recovery, and food industry [36, 31, 35]. The most popular computational methods for CFD simulations are based on the direct discretization of the Navier-Stokes equations using appropriate numerical methods, e.g. finite differences, finite volumes or finite elements [19]. They are usually difficult to implement and require large computer resources as well as some tedious preprocessing of the input data (e.g. generation and storage of complex computational grids). In this context, the mesoscopic Lattice Boltzmann Method (LBM), based on the kinetic theory of gases, has recently been gaining more and more attention as a versatile and simple fluid solver that offers a wide range of potential applications [26].

---

\*maciej.matyka@uwr.edu.pl

One of the main limitations of the original LBM algorithm is a relatively high computer memory demand, as one has to store the distribution function for all fluid nodes. This limits the size of the samples that can be simulated in a single machine. Also, an increased number of memory accesses and complex memory access patterns in the propagation of distribution function may form a bottleneck for parallel acceleration of the LBM [30]. It was shown that in a GPU implementation the efficiency of an LBM solver saturates with the filling memory fraction [11]. Therefore, much research has been focused on improving memory efficiency of the LBM algorithm, including modifications of the main LBM algorithm [2, 23] or data format and algorithms for sparse environments where most of the cells are getting fully blocked by obstacles [29, 32].

Here I test a memory-saving formulation of the simplified (fixed viscosity) LBM method done for flows with the relaxation time  $\tau = 1$ . In the standard LBM BGK algorithm the relaxation time  $\tau$  may range from nearly 1/2 up to 1 (highly viscous flows), however, the choice  $\tau = 1$  is a popular choice for single relaxation time BGK approximation [33, 20, 12]. For example,  $\tau = 1$  was chosen in the gray LBM model used for porous media flows [6], to compute first predictor step and fictitious viscosity solution in the simulation of the mold filling process [28], in the LBM multicomponent flow simulation with comparison to Finite Volume Methods [21], the immersed-boundary LBM for particles suspended in fluids [17]. It was shown that the value of  $\tau$  influences the accuracy of the LBM solver in flow through narrow pores and  $\tau = 1$  case was in the best agreement with advanced multi-relaxation time schemes [18, 20]. This is also a special case for multiphase flows where EDM (Exact Difference Method) agrees well with the Shan-Chen method in terms of measured gas density error (which is minimum at  $\tau = 1$  for the Shan-Chen model) [13]. Moreover, it was reported as the best choice for the Shan-Chen two immiscible fluid simulation [9]. Also, it was shown that setting  $\tau = 1$  in BGK LBM provides optimal accuracy in time if solutions are compared to direct Navier-Stokes equations [34]. Setting  $\tau = 1$  is also crucial for the fractional step formulation of LBM for high Reynolds flows [25].

Here I fix the viscosity of the model and set the relaxation time to  $\tau = 1$  (thus I will use the codename LBM1) and then modify the original LBM algorithm to a simpler, more compact and memory-efficient method. I provide a complete algorithm and test it against Poiseuille flow with error scaling analysis. Then I continue the test with Driven Cavity flows at varying Reynolds number and give criteria to calculate grid size necessary for stable simulations. Finally, I show that this approach leads to a significant memory drop and analyze this effect for various conditions and LBM models.

## 2 The Model

The Lattice Boltzmann Method use the multi-dimensional velocity distribution  $f_k(\mathbf{x}, t)$  to describe the state of the fluid. Function  $f_k(\mathbf{x}, t)$  corresponds to the probability that a molecule at position  $\mathbf{x}$  at time  $t$ , is moving with velocity  $\mathbf{e}_k$ . The original LBM algorithm consists of two steps: propagation and relaxation of the distribution function. It may be written as a discrete analogon to the Boltzmann transport equation (here with a linear approximation for the collision term) [8]:

$$f_k(\mathbf{x} + \mathbf{e}_k, t + 1) = f_k(\mathbf{x}, t) - \frac{f_k(\mathbf{x}, t) - f_k^{eq}(\mathbf{x}, t)}{\tau}, \quad (1)$$

where  $k$  is the direction on the lattice,  $f_k^{eq}$  is the equilibrium distribution function,  $\mathbf{e}_k$  is the lattice vector and  $\tau$  is the relaxation time. By varying  $\tau$ , the kinematic viscosity of the fluid may be controlled [8]

$$v = c_s^2 (\tau - 0.5), \quad (2)$$

where  $c_s$  is the sound speed (dependent on the variant of the model, e.g.  $c_s = 1/\sqrt{3}$  for two dimensional D2Q9 model [8]). The equilibrium  $f_k^{eq}$  is expressed in terms of macroscopic density  $\varrho$  and velocity  $\mathbf{u}$  of the flow field [5]:

$$f_k^{eq} = \omega_k \varrho \left( 1 + 3\mathbf{e}_k \cdot \mathbf{u} + \frac{9}{2}(\mathbf{e}_k \cdot \mathbf{u})^2 - \frac{3}{2}\mathbf{u}^2 \right), \quad (3)$$

where  $\omega_k$  are direction weights. Here, to include body force we may modify directly the momentum used for calculation of equilibrium (see e.g. [27]). To solve the fluid flow problem with the above equations we need to compute the macroscopic variables. The following sums over the distribution function let us compute the density and the velocity:

$$\varrho(\mathbf{x}, t) = \sum_k f_k(\mathbf{x}, t), \quad (4)$$

$$\mathbf{u}(\mathbf{x}, t) = \sum_k \mathbf{e}_k f_k(\mathbf{x}, t). \quad (5)$$

To save computer memory and eliminate the distribution function, we will first fix the relaxation time at  $\tau = 1$  [24, 37]. With this assumption the transport equation (see Eq. (1)) simplifies to:

$$f_k(\mathbf{x} + \mathbf{e}_k, t + 1) = f_k^{eq}(\mathbf{x}, t). \quad (6)$$

Now, instead of keeping the values of  $f_k$  in memory, we plug this equation in (4) and (5). Thus, a new formulation will consist of computing macroscopic fields from the equilibrium distribution only

$$\varrho(\mathbf{x}, t)|_{\tau=1} = \sum_k f_k^{eq}(\mathbf{x} + \mathbf{e}_k, t), \quad (7)$$

$$\mathbf{u}(\mathbf{x}, t)|_{\tau=1} = \sum_k f_{ik}^{eq}(\mathbf{x} + \mathbf{e}_k, t) \cdot \mathbf{e}_k. \quad (8)$$

where  $f^{eq}$  is the Maxwell-Boltzmann distribution defined before. With the above two equations, we can write down an algorithm in which step by step the equilibrium distribution is computed from the macroscopic velocity and density and then use these values to make another iteration. In this way, the storage of  $f_k$  can be now eliminated from the algorithm (see the next section).

For simplicity, henceforth I restrict our discussion to the D2Q9 model [8] (a two dimensional LBM model with nine lattice velocities  $\mathbf{e}_k$ ), where

$$\mathbf{e}_k \in \{(0, 0), (1, 0), (0, 1), (-1, 0), (0, -1), (1, 1), (-1, 1), (-1, -1), (1, -1)\}, \quad (9)$$

for  $k = 0 \dots 8$  respectively.

To complete the picture, we need to account for the boundary conditions at the no-slip (zero tangent velocity) walls. For fluid nodes located next to a

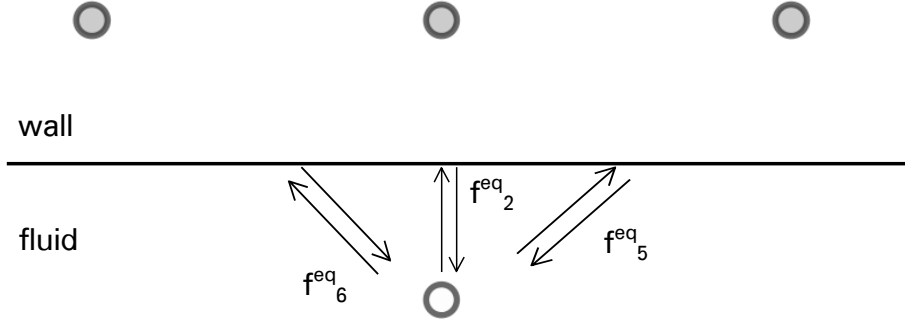


Figure 1: Calculation of the equilibrium function next to the no-slip wall.

no-slip wall the normal components of the equilibrium distribution function must be reversed (see Fig. 1) and used in equations (7) and (8). If we are at fluid node at  $\mathbf{x}$  and the node  $\mathbf{x} + \mathbf{e}_k$  is of the no-slip type (a solid wall) we must use the following expression for  $f_{ik}^{eq}$  in Eqs. (7) and (8)

$$f_{ik}^{eq}(\mathbf{x} + \mathbf{e}_k) = f_k^{eq}(\mathbf{x}, u = 0, v = 0) = \omega_k \cdot \varrho(\mathbf{x}). \quad (10)$$

For example, for the wall located at the north, we need to reverse three populations that move towards the wall:  $f_6^{eq}(\mathbf{x})$ ,  $f_2^{eq}(\mathbf{x})$  and  $f_5^{eq}(\mathbf{x})$  (see Fig. 1). Thus, for the north wall being no-slip we will have

$$\varrho_{\tau_1}(\mathbf{x}, t) = f_3^{eq}(\mathbf{x} + \mathbf{e}_1) + f_1^{eq}(\mathbf{x} + \mathbf{e}_3) + f_2^{eq}(\mathbf{x} + \mathbf{e}_4) + f_6^{eq}(\mathbf{x} + \mathbf{e}_8) + f_5^{eq}(\mathbf{x} + \mathbf{e}_7) + f_6^{eq}(\mathbf{x}) + f_2^{eq}(\mathbf{x}) + f_5^{eq}(\mathbf{x}). \quad (11)$$

The first five terms on the right-hand side in the above equation are standard incoming populations from neighboring nodes, whereas the three last terms are the populations reflected from the northern wall and computed in-place at the node  $\mathbf{x}$ . This procedure is used for all nodes adjacent to the walls. However, we do not need to write down an explicit expression for each orientation of the wall - it may be implemented by a simple expression in the algorithm. One has to check if the neighboring node is a wall or not and choose Eq. (3) or (10) accordingly.

## 2.1 The LBM1 algorithm

Using the derivation of the method in the previous section and Eqs. (7) and (8), I formulate a complete algorithm for the solver. Here  $R_c$ ,  $U_c$  and  $V_c$  are the macroscopic density, velocity (x) and velocity (y) components, respectively. Subscript  $c$  equal to 0 or 1 denotes the grid number (we are keeping two copies of the grid to ping-pong data in the memory). Variables  $i$ ,  $j$  and  $i_p$ ,  $j_p$  are grid coordinates. Within the algorithm, we use the macroscopic density, velocity, lattice vector components  $e_{k,x}$  and  $e_{k,y}$  and the grid direction weights  $\omega_{ik}$  to calculate the equilibrium distribution function  $f_{ik}^{eq}$ .

The algorithm starts with the initialization of macroscopic fields. At this point, we set up the flags for each node (flags denote if the node is occupied by fluid or solid). Also, the initial velocity and density fields are set up here (we start from zero velocity condition and density set to one). Next, we start the main loop over all fluid nodes (line 2) and for each of them compute the equilibrium distribution function from the local velocity and density. We also include the body force (lines 12-13 of the Algorithm 1). In the case of solid walls, we compute the equilibrium function by reflecting its normal components and assume zero velocity (no-slip boundary condition, line 17). Finally, we update the density and velocity by adding the populations that are incoming or being reflected from neighboring cells (lines 20-22). Implementation of this algorithm is straightforward - it contains  $D + 1$  tables (where  $D$  is the dimension of the model), two loops and one conditional (see the exemplary C/C++ implementation in A).

## 3 Validation and Results

To verify the solver I run the steady-state flow in a straight rectangular two-dimensional channel first. I use the periodic conditions at the left and right system edges and the no-slip at the top and bottom walls. The external body force  $f = 2.5 \cdot 10^{-5}$  (lattice units) was used to generate a steady flow along the channel axis. I used a grid of size of  $200 \times 100$ . To verify if the steady-state was reached I monitored the changes of velocity in the middle

---

**Algorithm 1** Complete time step of the LBM1 algorithm.

---

```

initialize flags and fields for fluid and solid nodes
for all fluid nodes (i, j) do
   $U_c(i, j) \leftarrow 0$ 
   $V_c(i, j) \leftarrow 0$ 
5:   $R_c(i, j) \leftarrow 0$ 
  for all directions k do
     $i_p \leftarrow i + e_{k,x}$  (neighbour in the direction k)
     $j_p \leftarrow j + e_{k,y}$ 
     $i_k \leftarrow$  direction inverse to k
10:  if  $(i_p, j_p)$  is fluid node then
     $r \leftarrow R_{1-c}(i_p, j_p)$ 
     $u \leftarrow (U_{1-c}(i_p, j_p) + f_x) / r$ 
     $v \leftarrow (V_{1-c}(i_p, j_p) + f_y) / r$ 
     $f_{ik}^{eq} \leftarrow \omega_{ik} r$ 
15:     $(1 - \frac{3}{2}(u^2 + v^2) + 3(e_{ik}^x u + e_{ik}^y v) + \frac{9}{2}(e_{ik}^x u + e_{ik}^y v)^2)$ 
    else
     $f_{ik}^{eq} \leftarrow \omega_k R_{1-c}(i, j)$ 
    end if
  end for
20:   $R_c(i, j) \leftarrow R_c(i, j) + f_{ik}^{eq}$ 
     $U_c(i, j) \leftarrow U_c(i, j) + e_{ik}^x f_{ik}^{eq}$ 
     $V_c(i, j) \leftarrow V_c(i, j) + e_{ik}^y f_{ik}^{eq}$ 
  end for
Visualization (optional)

```

---

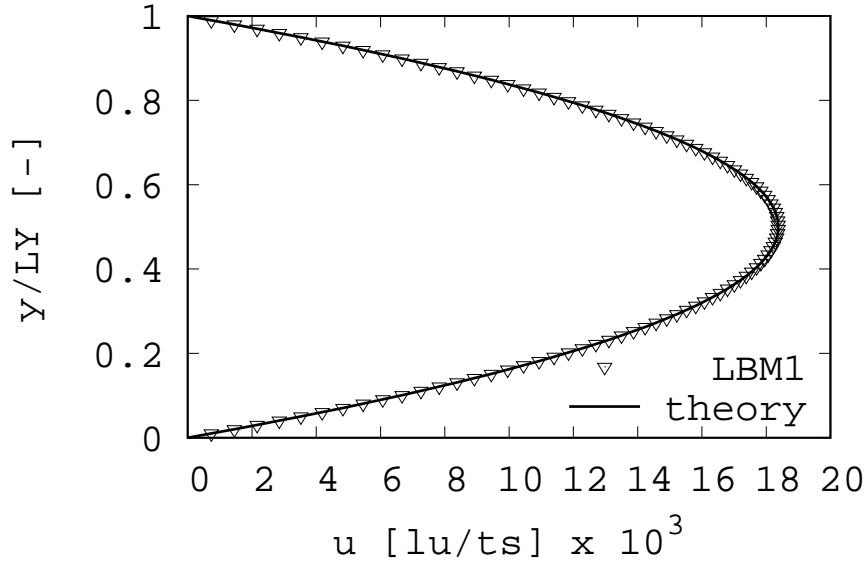


Figure 2: The velocity profile in the Poiseuille Flow simulated using the LBM1 algorithm (points) compared to the analytical solution (solid line). The profile was taken along the  $y$ -axis perpendicular to the flow direction.

of the channel and used the convergence condition:

$$\frac{|u_{n-1} - u_n|}{|u_n|} < \varepsilon, \quad (12)$$

where  $\varepsilon = 10^{-7}$ . The resulting velocity profile along the channel cross-section is given in Fig. 2. I find an excellent agreement between the numerical and analytical solutions. To quantify the agreement I repeat the simulations at varying grid size  $L$  and calculate the percentage error of the solution  $e = 100 \cdot \frac{|u - \tilde{u}|}{|\tilde{u}|}$ , where  $\tilde{u}$  is the analytical value of velocity in the middle of the channel. I find that the error follows the power law and scales with the grid size as  $L^{-2}$  (see Fig. 3).

Next, I used the standard Driven Cavity problem in which the fluid is enclosed in a rectangular cavity with a top lid moving at a constant velocity [4]. The Dirichlet boundary condition  $\mathbf{v}_{\text{lid}} = (u_0, 0)$  at the top boundary is applied. The no-slip condition is applied at the left, right and bottom boundaries. I performed the simulation on a  $1100 \times 1100$  grid and velocity  $u_0 = 0.4844$  at  $\text{Re}=3200$ . The simulation was continued at least until relative changes in the volumetric flux across vertical cross-section located at half of the system were smaller than 1%. I checked the change between two timesteps at  $\Delta t = 1000$  interval. In Fig. 4 we draw the streamlines on top of the final velocity field. The main vortex in the middle of the cavity, as well

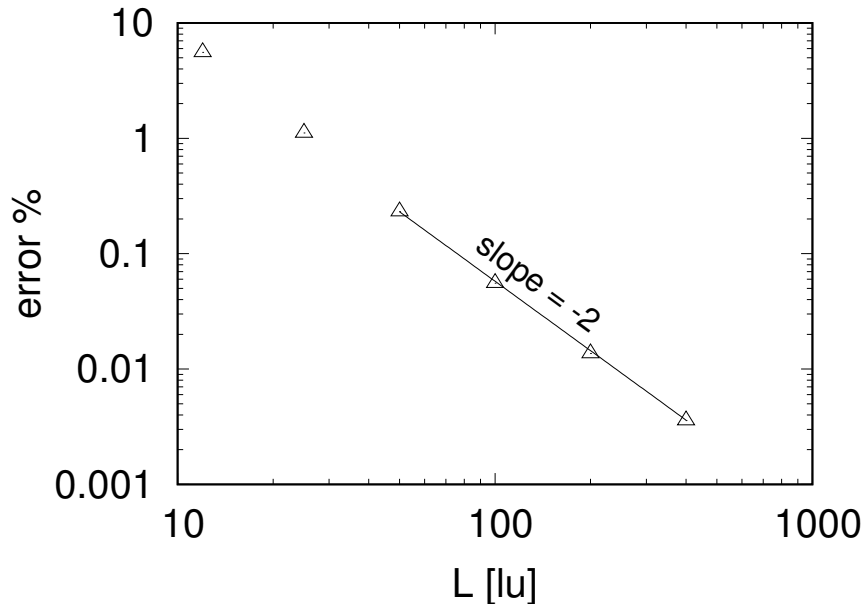


Figure 3: Scaling of the relative error between LBM1 and analytical solution (Poiseuille Flow). The solid line represent best fit to  $L^{-2}$  scaling taken at  $L \geq 40$ .

as vortex structures in corners of the cavity, are visible. The quantitative comparison with the multigrid method [7] is given in Fig. 5.

## 4 Discussion

In this paper a memory-saving algorithm for a simplified (fixed viscosity) LBM method is formulated and tested for flows with the relaxation time  $\tau = 1$ . This results in an immediate relaxation of the local distribution function [24] and put some limitations on the range of parameters that may be used in the model. The Reynolds number is defined as

$$Re = u_0 L / \mu, \quad (13)$$

where the viscosity  $\mu = 1/6$  (see Eq. 2). By changing  $u_0$  or  $L$  we control the Reynolds number which is now limited by the resolution of the grid only. To understand the limit we may estimate the Courant-Friedrichs-Lewy (CFL) condition. For velocity measured in the lattice units per time step we require, that  $u_0$  (velocity of the top lid) fulfill  $u_0 \ll 1$ . Taking small  $u_0$  stabilizes simulation, but at the same time slows down computation and require more memory as larger grids are required ( $u_0$  and  $L$  are the only parameters that

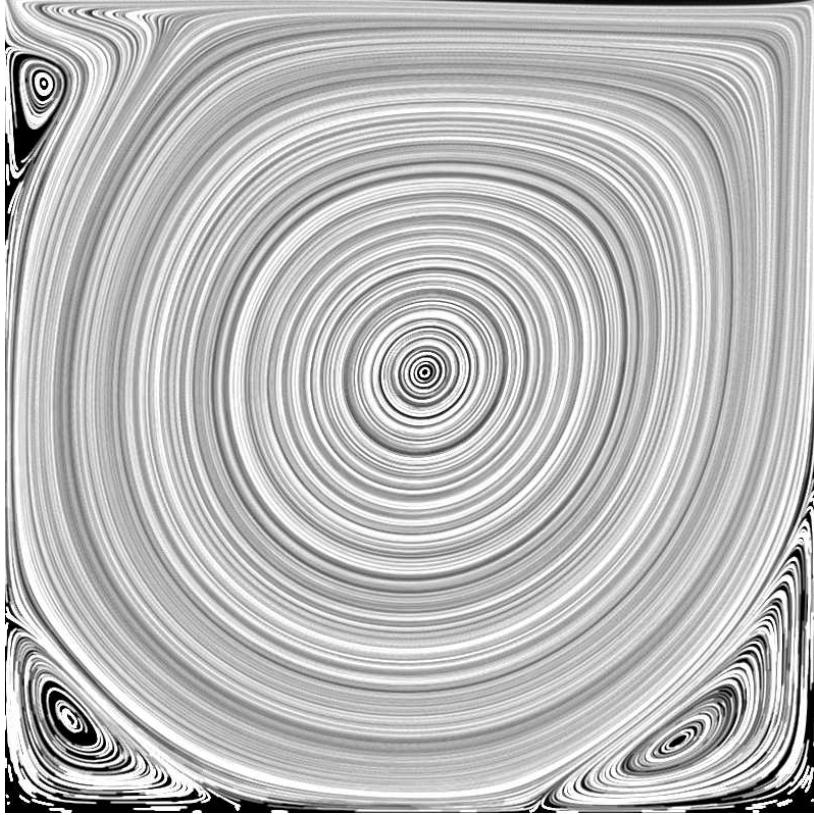


Figure 4: The driven cavity at  $Re=3200$  calculated using the LBM1 code on a  $1100 \times 1100$  grid. Visualization was made using massless tracers advected on top of the velocity field.

may be changed in Eq. 13). If we write the CFL condition as

$$u_0 = (Re/L) \cdot \mu \ll 1, \quad (14)$$

and because  $\mu = 1/6$ , to fulfill CFL criteria we should keep  $Re/L \ll 6$ . To check and validate this condition I run a series of simulations for the driven cavity at  $L$  from 50 to 1000 for increasing Reynolds number. If the simulation become unstable (and the solver crashed) after at least 1000 time steps, then the previous  $Re$  is taken as the maximum possible for given lattice size. Here, the simulation was not continuous until the final steady state. I repeated the procedure for various  $\tau$  and collect the data in Fig. 6. The data for the smallest viscosity and  $L < 100$  agrees with [16]. I notice that the lower relaxation time  $\tau$  is, the higher Reynolds number may be achieved. However, for the relaxation time  $\tau = 0.55$  the low resolution of the lattice leads to an inaccuracy in the solutions, especially in the regions where small vortices appear and in the center of main vortex (data not shown). I found

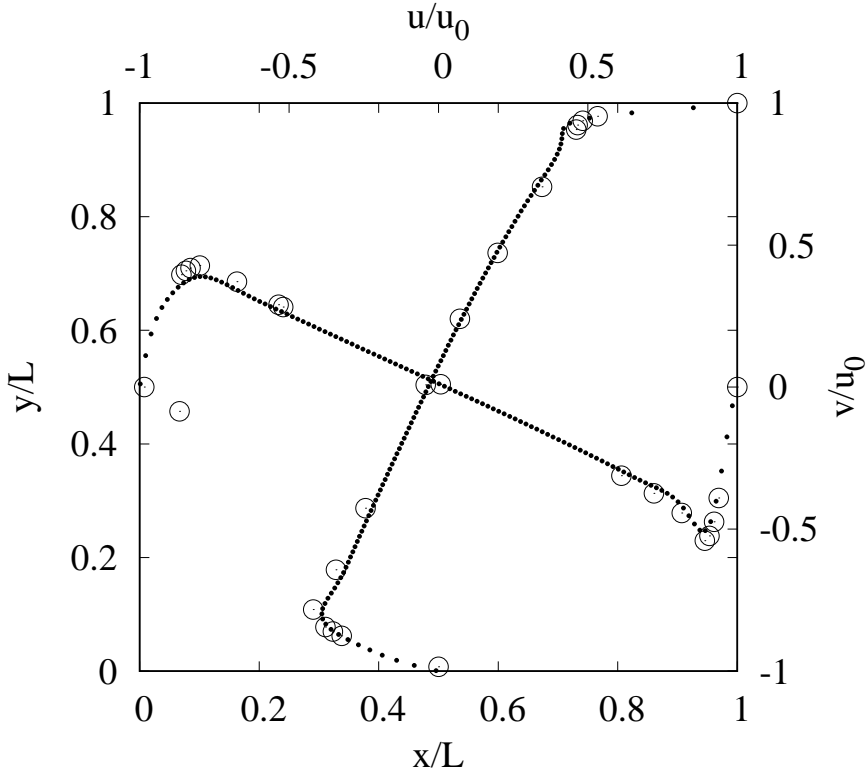


Figure 5: Velocity profiles in driven cavity at  $Re = 3200$ . LBM1 results (solid dots) are compared to the literature benchmark data [7] (open circles).

that if we keep  $\tau = 1$  then all converged solutions are of acceptable accuracy (see e.g. Fig. 5). This finding agrees with the conclusions based on the linear stability theory where  $\tau = 1$  was suggested, too[34]. In practice, one could estimate the maximum Reynolds number using the grid size  $L$  directly from the plot in Fig. 6 or from an empirical function fit to  $Re(L) = aL^b$  given in the figure caption. The results for  $Re=3200$  (see Fig. 5) confirm the stability of the solver. There is only one outlier point for  $u$  velocity component at  $x \approx 0.46$  that has probably been a typo in the original tables provided in [7].

The main advantage of a new formulation is its relatively low memory consumption. For example, if we use the AB lattice access pattern in standard LBM (where an additional copy of the main lattice is kept in memory) the memory consumption is estimated from [1]

$$M_{\text{LBM}} = (2Q + N_f)c, \quad (15)$$

where  $Q$  represents lattice velocity directions (i.e.  $Q=9$  in the standard D2Q9 model),  $N_f$  is the number of macroscopic fields (density, velocity, etc.) and  $c$  are bytes per single number ( $c = 4$  for float,  $c = 8$  for double-precision

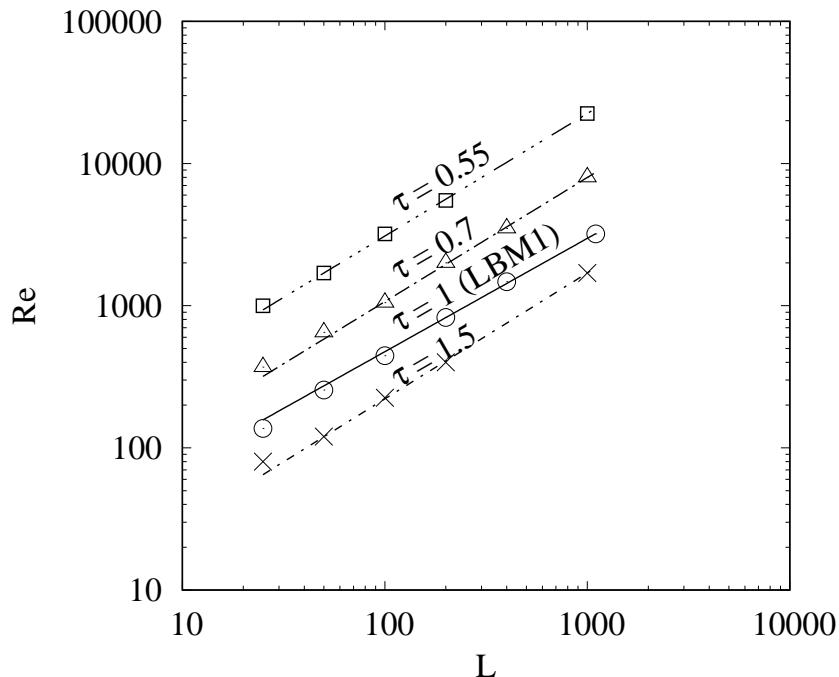


Figure 6: The maximum Reynolds number achieved at grid size  $L$  at various  $\tau$ . The data were obtained empirically by running several simulations for a given grid size. The least square fits (solid and dashed lines) to functions of the type  $Re(L) = aL^b$  gave:  $a=3.7$ ,  $b=0.89$  for  $\tau = 1.5$ ,  $a=12$ ,  $b=0.8$  for  $\tau = 1$ ,  $a=19$ ,  $b=0.87$  for  $\tau = 0.7$  and  $a=43$ ,  $b=0.93$  for  $\tau = 0.55$ .

data). We may write that  $N_f = D + 1$ , where  $D$  is the dimension of the model ( $D$  components of velocity plus density). Thus, in our case, if we eliminate distribution function in the LBM1 algorithm, it will need only

$$M_{\text{LBM}_1} = 2N_f c \quad (16)$$

bytes of the memory (the factor 2 appears because we store two copies of the macroscopic fields - one from the current and one from the previous time step). In D2Q9 model  $N_f = 3$  and  $Q = 9$ . Thus, using equations (15) and (16) we have  $M_{\text{LBM}} = 21c$  and  $M_{\text{LBM}_1} = 6c$  respectively. This means the LBM1 algorithm needs  $\Delta M \approx 76\%$  less memory than original implementation. A similar calculation for three dimensional D3Q27 model gives  $\Delta M \approx 86\%$ . In practice, for the 2D  $1000 \times 1000$  Driven Cavity flow in Fig. 4 we need  $m = 1000 \cdot 1000 \cdot 84 = 84$  MB (megabytes) of memory in the standard LBM to store all simulation data. In LBM1, however, for the same grid size we used only  $m = 1000 \cdot 1000 \cdot 24 = 24$  MB. One should keep in mind, however, that in the basic LBM1 implementation this memory drop

is true for low Reynolds number flows only (see Fig. 6) as higher Reynolds number may be achieved at smaller grids in the standard LBM. This problem, however, may be solved using i.e. fractional step approach to for viscosity boost [25], which we leave for the future research.

I suggest that the LBM1 algorithm may provide a good starting point for fast and memory-efficient implementations of a solver in parallel environments, including graphics processors (GPUs), as the number of memory accesses decreases with decreasing memory demand of the main algorithm. However, to provide complete parallel implementation, one would need to consider memory access patterns used to compute macroscopic fields, which may not be the most efficient in the basic LBM1 implementation. That, however, is out of the scope of this paper and I leave it for future work.

## 5 Conclusions

The presented LBM1 version of the LBM algorithm outperforms the original algorithm and is useful in large scale, low Reynolds number flows. This is important especially in systems where the memory storage matters. This includes multiscale media e.g. porous and artery systems, where the flow at microscale correlates with macroscopic properties of the medium.

Finally, it is rather surprising, how simple it is to implement a basic version of the LBM1 solver. The main function consists of a few lines of a simple C code (see A). The ratio of the work needed to achieve useful results is relatively low, especially compared to any standard CFD solver. Thus, we believe, the solution provided in this paper may be also attractive in computational physics education. From practical point of view, the LBM1 algorithm discussed here should be useful in applications where the original BGK Lattice Boltzmann was combined with the relaxation time  $\tau = 1$ . For example, in [33, 12, 6, 28, 17, 13, 9, 34, 25, 3, 10, 14, 15, 22] it is possible to save more than 75% of the memory by using LBM1 described here.

## 6 Acknowledgments

I would like to thank Jonas Latt from the University of Geneva for discussions. Also, many remarks and first reading comments from Remigiusz Durka and Zbigniew Koza from the University of Wrocław were very helpful.

## A The LBM1 C code for Driven Cavity

```

1 float U[2][L][L], V[2][L][L], R[2][L][L];
2 int F[L][L];
3 const int ex[9]={0,1,0,-1,0,1,-1,-1,1};

```

```

4  const int ey[9]={0,0,1,0,-1,1,1,-1,-1};
5  const int inv[9]={0,3,4,1,2,7,8,5,6};
6  const float w[9]={4/9.,1/9.,1/9.,1/9.,1/9.,1/36.,1/36.,1/36.,
7  1/36.};
8  float U0=0.5;
9
10 void init()
11 {
12   for(int i=0; i<L ; i++)
13   for(int j=0; j<L ; j++)
14   {
15     U[0][i][j]=V[0][i][j]=0;
16     U[1][i][j]=V[1][i][j]=0;
17     R[0][i][j]=R[1][i][j]=1;
18     F[i][j]=0;
19
20     if(j==0 or i==0 or i==L-1) F[i][j] = 1;
21     if(j==L-1) U[0][i][j] = U[1][i][j] = U0;
22   }
23 }
24
25 void LBMTau1(int c)
26 {
27   float r,u,v,f;
28
29   for(int i=0; i<L; i++)
30   for(int j=0; j<L-1; j++)
31   if(F[i][j]==0)
32   {
33     U[c][i][j]=V[c][i][j]=R[c][i][j]=0;
34
35     for(int k=0; k<9; k++)
36     {
37       int ip=i+ex[k], jp=j+ey[k], ik=inv[k];
38
39       if(F[ip][jp]==0)
40       {
41         r=R[1-c][ip][jp];
42         u=U[1-c][ip][jp]/r;
43         v=V[1-c][ip][jp]/r;
44
45         f=w[ik]*r*(1-(3/2.)*(u*u+v*v))+3.*(ex[ik]*u+ey[ik]*v)
46         +(9/2.)*(ex[ik]*u+ey[ik]*v)*(ex[ik]*u+ey[ik]*v));
47       }

```

```

48   else
49       f=w[ik]*R[1-c][i][j];
50
51       R[c][i][j] += f;
52       U[c][i][j] += ex[ik]*f;
53       V[c][i][j] += ey[ik]*f;
54   }
55 }
56 }

```

## References

- [1] Sailfish manual. <http://sailfish.us.edu.pl/simulation>, 2019. Accessed: 2019-10-04.
- [2] R. Argentini, A. Bakker, and C. Lowe. Efficiently using memory in lattice boltzmann simulations. *Future Generation Computer Systems*, 20(6):973–980, 2004.
- [3] R. Blaak and P. M. Sloot. Lattice dependence of reaction-diffusion in lattice boltzmann modeling. *Computer Physics Communications*, 129(1-3):256–266, 2000.
- [4] O. Botella and R. Peyret. Benchmark spectral results on the lid-driven cavity flow. *Computers & Fluids*, 27(4):421–433, 1998.
- [5] J. Buick and J. Cosgrove. Investigation of a lattice boltzmann model with a variable speed of sound. *Journal of Physics A: Mathematical and General*, 39(44):13807, 2006.
- [6] Y. Chen and K. Zhu. A study of the upper limit of solid scatters density for gray lattice boltzmann method. *Acta Mechanica Sinica*, 24(5):515–522, 2008.
- [7] U. Ghia, K. N. Ghia, and C. Shin. High-re solutions for incompressible flow using the navier-stokes equations and a multigrid method. *Journal of computational physics*, 48(3):387–411, 1982.
- [8] Z. Guo and C. Shu. *Lattice Boltzmann Method and Its' Applications in Engineering*. Advances in Computational Fluid Dynamics. World Scientific Publishing Company Incorporated, 2013.
- [9] F. Hai-Ping, W. Rong-Zheng, and F. Le-Wen. Lattice boltzmann method simulation on the flow of two immiscible fluids in complex geometry. *Chinese Physics*, 9(7):515, 2000.

- [10] I. Halliday, S. Lishchuk, T. Spencer, G. Pontrelli, and C. Care. Multiple-component lattice boltzmann equation for fluid-filled vesicles in flow. *Physical Review E*, 87(2):023307, 2013.
- [11] M. Januszewski and M. Kostur. Sailfish: A flexible multi-gpu implementation of the lattice boltzmann method. *Computer Physics Communications*, 185(9):2350–2368, 2014.
- [12] S. Khajepour, J. Cui, M. Dewar, and B. Chen. A study of wall boundary conditions in pseudopotential lattice boltzmann models. *Computers & Fluids*, 193:103896, 2019.
- [13] D. Lycett-Brown and K. H. Luo. Multiphase cascaded lattice boltzmann method. *Computers & Mathematics with Applications*, 67(2):350–362, 2014.
- [14] M. Matyka, A. Khalili, and Z. Koza. Tortuosity-porosity relation in porous media flow. *Phys. Rev. E*, 78(2):026306, 2008.
- [15] M. Mendoza, H. J. Herrmann, and S. Succi. Lattice boltzmann model for electronic structure simulations. In *Journal of Physics: Conference Series*, volume 640, page 012018. IOP Publishing, 2015.
- [16] A. Montessori, G. Falcucci, P. Prestininzi, M. La Rocca, and S. Succi. Regularized lattice bhatnagar-gross-krook model for two-and three-dimensional cavity flow simulations. *Physical Review E*, 89(5):053317, 2014.
- [17] L. Mountrakis, E. Lorenz, and A. Hoekstra. Revisiting the use of the immersed-boundary lattice-boltzmann method for simulations of suspended particles. *Physical Review E*, 96(1):013302, 2017.
- [18] C. Pan, L.-S. Luo, and C. T. Miller. An evaluation of lattice boltzmann schemes for porous medium flow simulation. *Computers & fluids*, 35(8-9):898–909, 2006.
- [19] J. Peiró and S. Sherwin. *Finite Difference, Finite Element and Finite Volume Methods for Partial Differential Equations*, pages 2415–2446. Springer Netherlands, Dordrecht, 2005.
- [20] P. Rao and L. Schaefer. Lattice boltzmann models for microtomographic pore-spaces. *Computers & Fluids*, 193:104294, 2019.
- [21] O. Shardt. Comparison of finite volume and lattice boltzmann methods for simulations of multicomponent flows. In *2019 AIChE Annual Meeting*. AIChE, 2019.

- [22] O. Shardt. Comparison of finite volume and lattice boltzmann methods for multicomponent flow simulations. *The Canadian Journal of Chemical Engineering*, 98:44–53, 2020.
- [23] M. Sheida, M. Taeibi-Rahni, and V. Esfahanian. A new approach to reduce memory consumption in lattice boltzmann method on gpu. *Journal of Applied Fluid Mechanics*, 10(1):55–67, 2017.
- [24] a. K. G. E. Shiyi Chen, Gary D. Doolen. Lattice-boltzmann fluid dynamics versatile tool for multiphase and other complicated flows. *Los Alamos Science*, (22):98–111, 1994.
- [25] C. Shu, X. Niu, Y.-T. Chew, and Q. Cai. A fractional step lattice boltzmann method for simulating high reynolds number flows. *Mathematics and Computers in Simulation*, 72(2-6):201–205, 2006.
- [26] S. Succi and S. Succi. *The Lattice Boltzmann Equation: For Complex States of Flowing Matter*. Oxford University Press, 2018.
- [27] M. C. Sukop and D. T. J. Thorne. *Lattice Boltzmann Modeling: An Introduction for Geoscientists and Engineers*. Springer Publishing Company, Incorporated, 1 edition, 2007.
- [28] M. Szucki, J. Suchy, J. Lelito, P. Malinowski, and J. Sobczyk. Application of the lattice boltzmann method for simulation of the mold filling process in the casting industry. *Heat and Mass Transfer*, 53(12):3421–3431, 2017.
- [29] T. Tomczak and R. G. Szafran. Sparse geometries handling in lattice boltzmann method implementation for graphic processors. *IEEE Transactions on Parallel and Distributed Systems*, 29(8):1865–1878, 2018.
- [30] T. Tomczak and R. G. Szafran. A new gpu implementation for lattice-boltzmann simulations on sparse geometries. *Computer Physics Communications*, 235:258–278, 2019.
- [31] Y. Toparlak, B. Blocken, B. Maiheu, and G. Van Heijst. A review on the cfd analysis of urban microclimate. *Renewable and Sustainable Energy Reviews*, 80:1613–1640, 2017.
- [32] P. Valero-Lara. Reducing memory requirements for large size lbm simulations on gpus. *Concurrency and Computation: Practice and Experience*, 29(24):e4221, 2017.
- [33] Y. Wei. Lattice boltzmann simulations for thermal vapor-liquid two-phase flows. *The Journal of Computational Multiphase Flows*, 4(1):103–109, 2012.

- [34] R. A. Worthing, J. Mozer, and G. Seeley. Stability of lattice boltzmann methods in hydrodynamic regimes. *Physical Review E*, 56(2):2243, 1997.
- [35] B. Xia and D.-W. Sun. Applications of computational fluid dynamics (cfd) in the food industry: a review. *Computers and electronics in agriculture*, 34(1-3):5–24, 2002.
- [36] F. J. Zajaczkowski, S. E. Haupt, and K. J. Schmehl. A preliminary study of assimilating numerical weather prediction data into computational fluid dynamics models for wind prediction. *Journal of Wind Engineering and Industrial Aerodynamics*, 99(4):320–329, 2011.
- [37] J. G. Zhou. Macroscopic lattice boltzmann method (maclab). *CoRR*, abs/1901.02716, 2019.